# Experimental Observation of Halo-Type Boundary Image Sticking in AC Plasma Display Panel

Choon-Sang Park, Heung-Sik Tae, *Senior Member, IEEE*, Young-Kuk Kwon, and Eun Gi Heo

***Abstract*—Infrared-emission observations show that the discharge characteristics related to the MgO surface are improved in both the image sticking and boundary image sticking cells, whereas luminance observations show a deterioration in the visible-conversion characteristics related to the phosphor layer in both the image sticking and boundary image sticking cells. Consequently, the image sticking phenomenon is strongly related to the Mg species sputtered from the MgO surface of the discharge cells due to an iterant strong sustain discharge. In particular, halo-type boundary image sticking is due to the redeposition of Mg species on both the MgO and phosphor layers in the nondischarge region adjacent to the discharge region, as confirmed by $V_t$ close curve, time-of-flight secondary ion mass spectrometry, and scanning electron microscope analyses.**

***Index Terms*—Halo-type boundary image sticking, redeposition of Mg species, scanning electron microscope (SEM) analyses, time-of-flight secondary ion mass spectrometry (TOF-SIMS), $V_t$ close curve, 42-in ac plasma display panel (PDP) module.**

## I. Introduction

THE REALIZATION of a high-quality plasma display panel (PDP) requires an urgent solution to the image sticking and image-retention problems induced in the PDP cells when strong sustain discharges have been repeatedly produced during a sustain period [1]–[4]. Image retention means a temporal image sticking that is easily recoverable, whereas image sticking means a permanent image sticking that is not recoverable. Image sticking is also sometimes induced in the nondischarge cells adjacent to the discharge cells, referred to as boundary image sticking [3], [4]. However, the detailed mechanism that induces image sticking and boundary image sticking was still not fully understood [5], [6]. In experimental results, the authors of this paper found that image sticking was strongly related to the Mg species sputtered from the magnesium-oxide (MgO) surface of the discharge cells due to the severe ion bombardment during a sustain discharge [7], [8]. Here, the Mg species just means a material including Mg component. The deposition of the sputtered Mg species on the phosphor layer of the discharge cells, or the redeposition of the sputtered Mg species on another MgO surface of the nondischarge cells adjacent to the discharge cells, may then alter the reset or sustain discharge characteristics, causing image sticking or boundary image sticking. Therefore, this paper examines the effects of the Mg species sputtered from the MgO surface on the image sticking phenomenon, particularly boundary image sticking in the nondischarge region adjacent to the discharge region. The firing voltage, luminance, and infrared (IR: 828 nm) emission of the nondischarge region adjacent to the discharge region are observed in comparison with those of the discharge region and nondischarge region far away from the discharge region using two different image patterns, a dark and full-white background, after displaying a square-type image (197 × 72 pixels) at peak luminance for about 500 h on a commercial 42-in PDP-TV with a high Xe (15%) content. A long operating time, such as 500 h, is chosen to produce an image sticking pattern including a boundary image sticking pattern that is not recoverable. In particular, a scanning electron microscope (SEM) image of the MgO surface and related time-of-flight secondary ion mass spectrometry (TOF-SIMS) are used to identify the change in the morphology of the MgO surface as a result of the iterant strong sustain discharge and the deposition or redeposition of the sputtered Mg species, respectively. Furthermore, the resultant changes in the firing voltage among the three electrodes are measured using the voltage threshold $(V_t)$ close curve technique [9]–[11].

Manuscript received January 5, 2007; revised March 19, 2007. This work was supported in part by the Regional Innovation Center Program (ADMRC) of the Ministry of Commerce, Industry and Energy of Korea and in part by the Brain Korea 21 (BK21). The review of this paper was arranged by Editor D. Verret.

C.-S. Park and H.-S. Tae are with the School of Electrical Engineering and Computer Science, Kyungpook National University, Daegu 702-701, Korea (e-mail: hstae@ee.knu.ac.kr).

Y.-K. Kwon and E. G. Heo are with the Plasma Display Panel Division, Samsung SDI Company Ltd., Chungchongnam-Do 330-300, Korea.

Color versions of one or more of the figures in this paper are available online at http://ieeexplore.ieee.org.

Digital Object Identifier 10.1109/TED.2007.896578

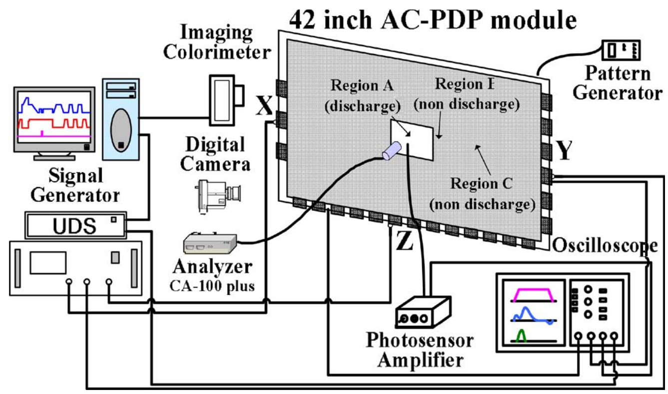


Fig. 1. Schematic diagram of experimental setup employed in this paper.

## II. Experimental Setup for Halo-Type Boundary Image Sticking in AC PDP

Fig. 1 shows the optical-measurement systems and commercial 42-in ac PDP module with three electrodes used in the

TABLE I
SPECIFICATIONS OF 42-in AC PDP USED IN THIS PAPER

| Front Panel | | Rear Panel | |
|---|---|---|---|
| ITO width | 225 μm | Barrier rib width | 55 μm |
| ITO gap | 85 μm | Barrier rib height | 120 μm |
| Bus width | 50 μm | Address width | 95 μm |
| Pixel Pitch | | 912 × 693 μm | |
| Gas chemistry | | Ne-Xe (15 %)-He (35 %) | |
| Barrier rib type | | Closed rib | |

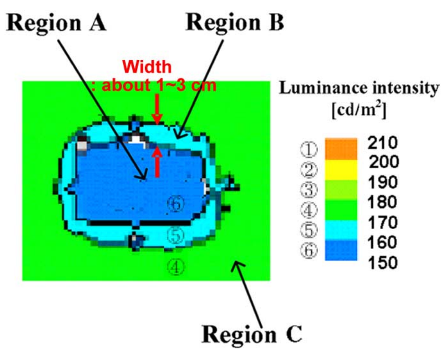


Fig. 2. Imaging pattern showing luminance difference among regions A, B, and C measured from 42-in panel using imaging colorimeter with full-white background: region A indicates image sticking cells, while region B indicates halo-type boundary image sticking cells.

experiment, where $X$ is the sustain electrode, $Y$ is the scan electrode, and $Z$ is the address electrode. A color analyzer (CA-100 plus), imaging photometer (Prometric PM Series), pattern generator, signal generator, and photo-sensor amplifier (Hamamatsu, C6386) were used to measure the luminance, IR emission, and $V_t$ close curve, respectively. To produce the boundary image sticking, the entire region of the 42-in panel was changed to a dark background (about 0.1 cd/m$^2$) or full-white background (about 175 cd/m$^2$) image immediately after displaying a square-type image (region A) at peak luminance (about 1000 cd/m$^2$) for about 500 h. The conventional driving method with a selective reset waveform was adopted. The frequency for the sustain period was 200 kHz, and the sustain voltage was 206 V (the detailed panel specifications are listed in Table I). Fig. 2 shows the imaging pattern, revealing the luminance difference among the regions A, B, and C when the entire region of the 42-in panel is changed to a full-white background immediately after displaying a square-type image (region A) at peak luminance for about 500 h. In the absence of any image sticking phenomenon, the luminance in Fig. 2 would be almost the same among the three regions A, B, and C. However, as shown in Fig. 2, the three regions exhibited a different luminance with the full-white background due to the image sticking induced by the iterant strong sustain discharge in region A. Even though no sustain discharge was produced in region B, the image sticking phenomenon was still observed, and since the region formed a circular shape, it was hereinafter referred to as "halo-type" boundary image sticking. The 23% area of the 42-in test panel employed in this research showed a good uniform characteristic for the luminance, i.e., the luminance uniformity of about less 2%. Within this area, the regions A (discharge region), B (boundary region),

TABLE II
CHANGES IN LUMINANCE IN REGIONS A, B, AND C
WITH OPERATING TIME

| Operating Time [hour] | Luminance [cd/m$^2$] | | |
|---|---|---|---|
| | Region A | Region B | Region C |
| 0 | 177.47 | 179.33 | 179.43 |
| 140 | 171.01 | 177.94 | 181.07 |
| 300 | 169.78 | 172.02 | 180.54 |
| 500 | 158.29 | 168.88 | 175.17 |

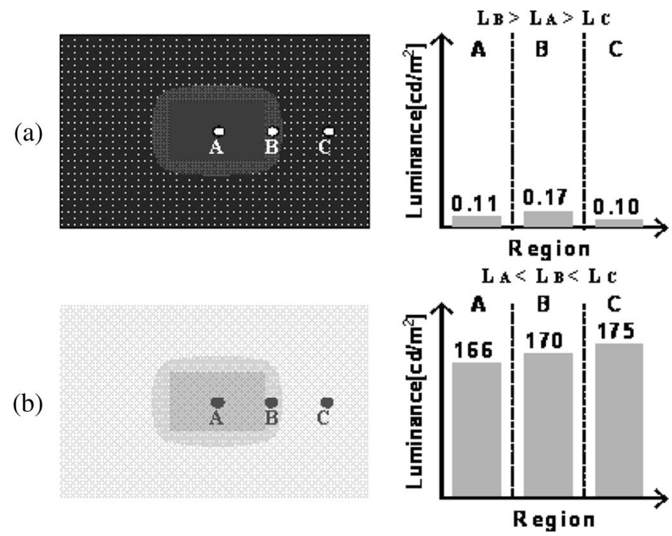


Fig. 3. Image sticking pattern with (a) dark background and (b) full-white background captured from 42-in panel where region A is discharge region, region B is nondischarge region adjacent to discharge region, and region C is nondischarge region far away from discharge region.

and C (nondischarge region) were chosen, and the corresponding luminance was measured in each region as a function of an operating time. The changes in the luminance for three regions A, B, and C with a variation of operating time from 0 to 500 h were measured and listed in Table II.

## III. EXPERIMENTAL OBSERVATION OF HALO-TYPE BOUNDARY IMAGE STICKING IN AC PDP

### A. *Monitoring of Luminance*

Fig. 3(a) and (b) shows the luminance difference among the regions A (discharge region), B (nondischarge region adjacent to the discharge region), and C (nondischarge region far away from the discharge region) observed with Fig. 3(a) a dark background and Fig. 3(b) full-white background after an iterant 500-h strong sustain discharge with a square-type image, as shown in Fig. 1. In Fig. 3(a), with the dark background, image sticking occurred in regions A and B. With the dark background produced by just a weak reset discharge, the luminance of region A (discharge region, i.e., image sticking cells) was higher than that of region C (nondischarge region), yet region B (nondischarge region adjacent to the discharge region) showed the highest luminance. As the brightest luminance of region B in Fig. 3(a) formed a circle, the image sticking in region B was called "halo-type boundary image sticking with

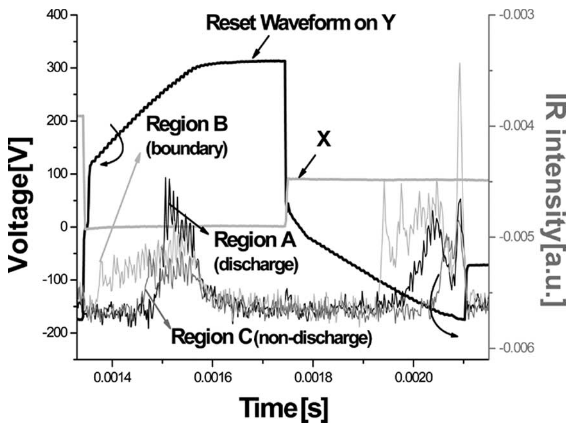


Fig. 4. Comparison of IR (828 nm) emissions measured from regions A, B, and C during reset period with dark background.

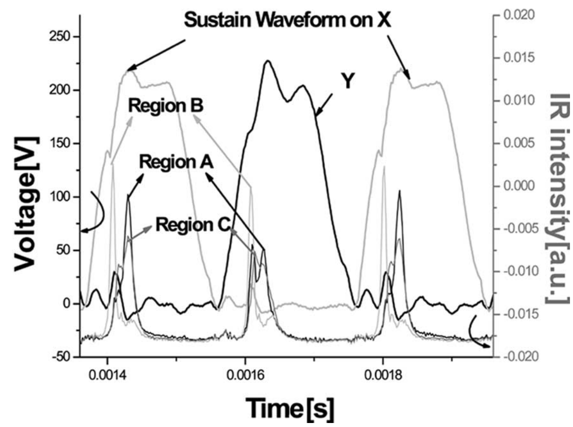


Fig. 5. Comparison of IR (828 nm) emissions measured from regions A, B, and C during sustain period with full-white background.

a dark background." As shown in Fig. 3(b), image sticking also occurred in regions A and B with a full-white background. Yet, unlike the case of a dark background, the luminance of region B was lower than that of region C, although higher than that of region A with the full-white background. The image sticking in region B was also called "halo-type boundary image sticking with a full-white background."

### *B. Monitoring of IR Emission*

Fig. 4 shows the changes in the IR (828 nm) emissions measured from regions A, B, and C during the reset period with a dark background produced by a weak reset discharge. The IR peak for region B was observed to be shifted to the left compared to that for regions A and C, indicating that the weak reset discharge was efficiently initiated at a lower starting discharge voltage during the reset period. At the forepart of the IR emission waveform produced dominantly by the $X{-}Y$ discharge (i.e., the surface discharge between the MgO layers), the halo-type boundary image sticking region (region B) showed the fastest IR emission and the discharge region (region A) showed the latest IR emission. However, at the back part of the IR-emission waveform produced dominantly by the $Z{-}Y$ discharge (i.e., the plate-gap discharge between the phosphor and MgO layers), the discharge region (region A) showed the most intensive IR emission peak, and the nondischarge region (region C) showed the weakest IR emission peak.

Meanwhile, Fig. 5 shows the changes in the IR (828 nm) emissions measured from regions A, B, and C during the sustain period to investigate the IR-emission characteristics with a full-white background. Fig. 5 shows a little asymmetric IR-emission intensities depending on applying the sustain waveform to the $X$- or $Y$-electrode, which is not related to the image sticking phenomenon. The IR-emission data in Fig. 5 revealed that the IR peaks for regions A and B were intensified compared to those for region C. However, the luminance characteristics in regions A and B were deteriorated with the full-white background, as shown in Fig. 3(b). The IR-emission characteristics are closely related to the MgO surface, whereas the luminance characteristics are more related to the visible-conversion capability of the phosphor layer. Consequently, the data in Figs. 3–5 indicated that the discharge characteristics were improved in the image sticking cells (discharge cells in region A) and boundary image sticking cells (nondischarge cells in region B), whereas the visible-conversion characteristics were aggravated in the image sticking cells (discharge cells in region A) and boundary image sticking cells (nondischarge cells in region B).

### *C. Monitoring of Firing Voltage Using $V_t$ Close Curve*

To investigate the reasons for the discrepancy in the IR emission and luminance characteristics for regions A and B with dark and full-white backgrounds, the $V_t$ close curves were measured in regions A, B, and C, respectively. Fig. 6 shows the $V_t$ close curves measured for regions A, B, and C without any initial wall charges, while Table III shows the discharge types for the six sides of the measured $V_t$ close curve and corresponding cathode conditions [8], [9]. As shown in Fig. 6 for region A, the firing voltages for sides V (plate-gap discharge between the $Y$ and $Z$ electrodes under phosphor-cathode conditions) and VI (plate-gap discharge between the $X$ and $Z$ electrodes under phosphor-cathode conditions) were remarkably decreased. In contrast, in region A, the firing voltages for sides I $(X{-}Y)$, II $(Z{-}Y)$, III $(Z{-}X)$, and IV $(Y{-}X)$ under MgO-cathode conditions were slightly increased. It is already known that the firing voltage under MgO-cathode conditions is much lower than that under phosphor-cathode conditions, as the secondary electron-emission characteristics of the MgO layer are much better than those of the phosphor layer. In region A, where an iterant strong sustain discharge was produced for 500 h, the discharge characteristics under phosphor-cathode conditions significantly improved, whereas the discharge characteristics under MgO-cathode conditions slightly deteriorated. Therefore, the significant reduction in the firing voltage under phosphor-cathode conditions in region A, as shown by the V and VI sides of the measured $V_t$ close curve in Fig. 6, confirmed that a large amount of Mg species with a higher secondary electron-emission coefficient was deposited on the phosphor layer. In this case, the Mg species on the phosphor layer was assumed to have been sputtered from the MgO surface of the cells, where the strong sustain discharge had been repeatedly produced. Even in region B, the firing voltage under phosphor-cathode

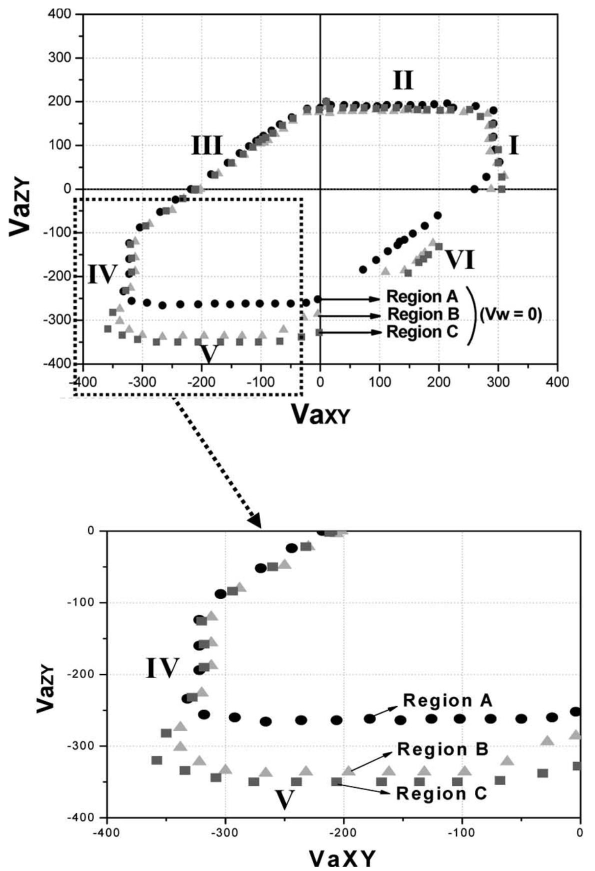


Fig. 6. Comparison of $V_t$ close curves measured for regions A, B, and C without initial wall charges.

TABLE III
SIX SIDES OF $V_t$ CLOSE CURVE IN FIG. 6 AND ASSOCIATED DISCHARGE TYPES

| Sides | Discharge type | Cathode/Anode |
|---|---|---|
| I | Surface discharge (X-Y) | MgO/MgO |
| II | Plate-gap discharge (Z-Y) | MgO/Phosphor |
| III | Plate-gap discharge (Z-X) | MgO/Phosphor |
| IV | Surface discharge (Y-X) | MgO/MgO |
| V | Plate-gap discharge (Y-Z) | Phosphor/MgO |
| VI | Plate-gap discharge (X-Z) | Phosphor/MgO |

conditions was decreased, although the variation in the voltage was not large compared to that in region A. Consequently, this result clearly showed that the Mg species sputtered from the MgO surface of the discharge cells (the cells in region A) was transported to the adjacent cells (the cells in region B) and contributed to reducing the firing voltage under phosphor-cathode conditions. Table IV shows the detailed changes in the firing voltages obtained from the $V_t$ close curves measured for regions A, B, and C. In region A, the reduced firing voltages, $\Delta V_{Y-Z}$ and $\Delta V_{X-Z}$, for the $Y-Z$ (side V) and $X-Z$ (side VI) discharges were about 100 and 80 V, respectively, whereas in region B, the reduced firing voltages, $\Delta V_{Y-Z}$, and $\Delta V_{X-Z}$, for the $Y-Z$ (side V) and $X-Z$ (side VI) discharges were about 10–15 and 5–10 V, respectively. Thus, as aforementioned, the reduction in the firing voltage for the plate-gap discharge under phosphor-cathode conditions was mainly due to the deposition of Mg species onto the phosphor layers, caused by

TABLE IV
DIFFERENCE IN FIRING VOLTAGE MEASURED FROM REGIONS A, B, AND C

| Sides | | Firing voltage | | |
|---|---|---|---|---|
| | | Region A | Region B | Region C |
| MgO Cathode | I | 292V | 284V | 290V |
| | II | 194V | 178V | 186V |
| | III | 218V | 206V | 210V |
| | IV | 322V | 312V | 318V |
| Phosphor Cathode | V | 262V | 336V | 350V |
| | VI | 258V | 324V | 332V |

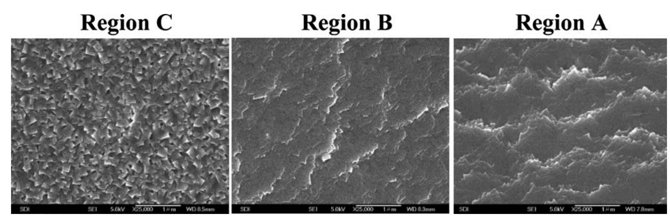


Fig. 7. Comparison of MgO-surface SEM images for regions A, B, and C.

the sputtering of MgO induced by an iterant strong sustain discharge. Meanwhile, in region A, the firing voltages under MgO-cathode conditions were increased by about 2–8 V, whereas in region B, the firing voltages under MgO-cathode conditions were decreased by about 4–8 V. Therefore, the $V_t$ close curve results showed that the decrease in the luminance of the image sticking cells (region A) could be attributed to the prohibition of a visible conversion from the vacuum ultraviolet (VUV) of the phosphor layers caused by MgO deposition onto the phosphor layers, instead of the deterioration of the phosphor layer itself. Furthermore, it would appear that the reduction in the luminance of the boundary image sticking cells (region B) was also due to the deposition of Mg species onto the phosphor layer, while the fast IR initiation in region B was due to the redeposition of Mg species onto the MgO layer. As such, this redeposition of Mg species onto both the MgO and phosphor layers caused the luminance difference trouble in the halo-type boundary image sticking cells (region B).

## *D. Monitoring of Deposition of Sputtered Mg Species on Phosphor Layer and MgO Layer*

To identify the Mg species deposited on the phosphor layer and MgO layer, the SEM and TOF-SIMS were used to inspect the surface morphology and analyze the deposited Mg species, respectively. Fig. 7 shows the SEM images captured for regions A, B, and C. Although, the cells in region B were nondischarge cells, their morphology was almost similar to that for the cells in the discharge region (region A). Theoretically, the morphology of the MgO surface should not change if the cells are not discharged. Nonetheless, a change was observed in the morphology of the MgO surface of the nondischarge cells (region B), presumably due to the redeposition of the MgO sputtered by the iterant strong sustain discharge in the discharge region A adjacent to the nondischarge region B. As shown in Table IV, the firing voltages under MgO-cathode conditions

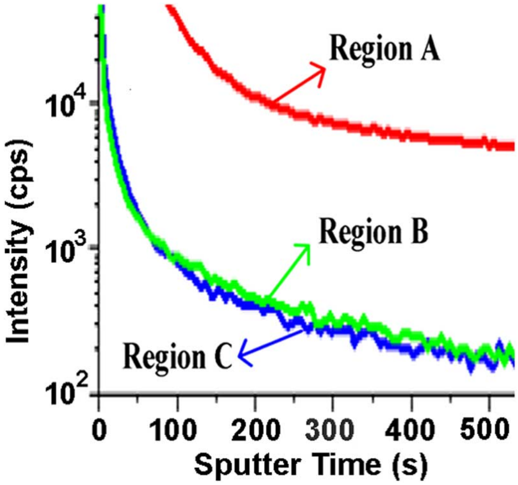


Fig. 8. Comparison of Mg-profiles of red phosphor layer for regions A, B, and C measured using TOF-SIMS analysis.

were decreased in region B, implying that the redeposition of MgO onto the MgO surface contributed to the lowering the firing voltage. Fig. 8 shows the comparison of the Mg-profiles on the red phosphor layer for regions A, B, and C using a TOF-SIMS analysis. In Fig. 8, the Mg profile meant the intensity of the Mg sputtered from the red phosphor layer over time when the Ar ions struck the surface of the red phosphor layer. As shown in Fig. 8, the Mg intensity in regions A and B shifted upward compared to that in region C, indicating that the Mg was redeposited onto the phosphor layer. Although the sputtered Mg species were predominantly redeposited in the discharge region A, there was also a slight redeposition in the nondischarge region B adjacent to the discharge region A. The redeposition of Mg on the phosphor layer significantly affected the discharge characteristics, particularly under phosphor-cathode conditions. Therefore, the firing voltage in region A, where the sputtered Mg species were predominantly redeposited, was observed to be the lowest, as shown in the $V_t$ close curve analysis in Fig. 6. Furthermore, the firing voltage in region B, where the sputtered Mg species were slightly redeposited, was observed to be lower than that in the nondischarge region C, where the sputtered Mg species were not redeposited. Thus, it was concluded that the redeposition of the Mg species onto both the MgO layer and the phosphor layer seemed to contribute to enhancing the discharge characteristics, such as the firing voltage and IR emission, yet the redeposition of Mg onto the phosphor layer deteriorated the visible-conversion efficiency of the phosphor layer from VUV, thereby lowering the luminance.

### *E. Monitoring of Chromaticity Coordinates and Color Temperature*

Table V shows the CIE chromaticity coordinates and related color temperatures measured for regions A, B, and C. As shown in Table V, the chromaticity coordinates, $x$ and $y$, were changed for both the image sticking cells (region A) and boundary image sticking cells (region B) relative to the normal cells without image or boundary image sticking (region C), where $\Delta x = 0.0039$ and $\Delta y = 0.0051$ for region A relative to region C, and $\Delta x = -0.0048$ and $\Delta y = -0.0084$ for

TABLE V
CIE (1931) CHROMATICITY COORDINATES AND COLOR TEMPERATURES MEASURED FROM REGIONS A, B, AND C

| | | Region A | Region B | Region C |
|---|---|---|---|---|
| Chromaticity coordinates | x | 0.3109 | 0.3022 | 0.3070 |
| | y | 0.3221 | 0.3086 | 0.3170 |
| Color temperature, T [K] | | 6667 | 7418 | 6953 |

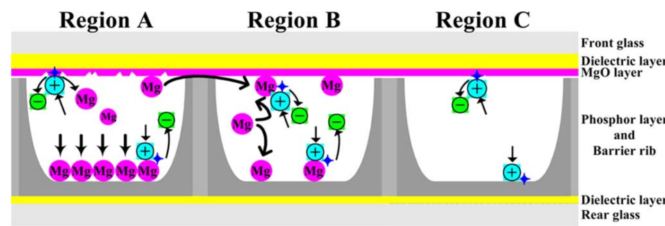


Fig. 9. Sputtering and redeposition schematic model of MgO layer protecting against accelerated ions.

region B relative to region C. The resultant color temperatures were also changed for both the image sticking cells (region A) and boundary image sticking cells (region B) in relation to the normal cells (region C), where $\Delta T = -286$ [K] for region A in relation to region C, and $\Delta T = 465$ [K] for region B in relation to region C. As aforementioned in the previous section, the results indicated a deterioration in the color-reproduction characteristics for both the image sticking and boundary image sticking cells due to the redeposition of Mg onto the phosphor layer.

### *F. Schematic-Mechanism Model for Describing the Image Sticking Phenomenon*

Based on the experimental results obtained using the $V_t$ close curve, SEM, and TOF-SIMS analyses, the schematic model shown in Fig. 9 revealed that the main cause of the image sticking problem was the sputtering of the MgO protective layer and resultant deposition or redeposition on the phosphor and MgO layers. In region A where the strong sustain discharge was repeatedly produced, Mg species were sputtered from the MgO surface due to the bombardment of ions onto the MgO-protecting layer during the iterant strong sustain discharge [7], thus the Mg species were predominantly redeposited on the phosphor layers of the cells in region A. Furthermore, the MgO surfaces in region A were changed into damaged MgO surfaces due to the severe ion bombardment, causing a slight increase in the firing voltage under MgO-cathode conditions. Meanwhile, the redeposition of the Mg species on the phosphor layer contributed to enhancing the plate-gap discharge, particularly under phosphor-cathode conditions, thereby increasing the IR emission during the reset period, and even during the sustain period. However, the redeposition of the Mg species on the phosphor layer prohibited the visible conversion of the phosphor layer, thereby decreasing the luminance.

In region B, with no sustain discharge yet located near region A, Mg species were transported from the adjacent cells where the MgO surface was sputtered and redeposited on the MgO surface and phosphor layer, respectively. The redeposited Mg species on both the MgO surface and the phosphor layer in region B then contributed to enhancing both the surface and plate-gap discharges, thereby increasing the IR emission during the reset and sustain periods. However, as in region A, the redeposition of the Mg species on the phosphor layer in region B prohibited the visible conversion of the phosphor layer, thereby decreasing the luminance.

## IV. Conclusion

After displaying a square-type image at peak luminance for about 500 h on a 42-in PDP-television (PDP-TV) with a high Xe (15%) content, the luminance and IR (828 nm) emission for the nondischarge region adjacent to the discharge region were observed in comparison with those for the discharge region and nondischarge region far away from the discharge region using two different image patterns, a dark and full-white background. In particular, halo-type boundary image sticking was observed in the nondischarge region adjacent to the discharge region. With the dark background, the IR was initiated the fastest and the luminance was the highest in the region adjacent to the discharge region, whereas with the full-white background, although the IR was still initiated the fastest in the region adjacent to the discharge region, its luminance was only higher than that of the discharge region and lower than that of the region far away from the discharge region. The $V_t$ close curves and SEM and TOF-SIMS analyses confirmed that the halo-type boundary image sticking phenomenon was due to the redeposition of MgO on both the MgO and phosphor layers in the nondischarge region adjacent to the discharge region.

## References

[1] H.-S. Tae, J.-W. Han, S.-H. Jang, B.-N. Kim, B. J. Shin, B.-G. Cho, and S.-I. Chien, "Experimental observation of image sticking phenomenon in AC plasma display panel," *IEEE Trans. Plasma Sci.*, vol. 32, no. 6, pp. 2189–2196, Dec. 2004.

[2] H.-S. Tae, C.-S. Park, B.-G. Cho, J.-W. Han, B. J. Shin, S.-I. Chien, and D. H. Lee, "Driving waveform for reducing temporal dark image sticking in AC plasma display panel based on perceived luminance," *IEEE Trans. Plasma Sci.*, vol. 34, no. 3, pp. 996–1003, Jun. 2006.

[3] J.-W. Han, H.-S. Tae, B. J. Shin, S.-I. Chien, and D. H. Lee, "Experimental observation of temperature-dependent characteristics for temporal dark boundary image sticking in 42-in. AC-PDP," *IEEE Trans. Plasma Sci.*, vol. 34, no. 2, pp. 324–330, Apr. 2006.

[4] J.-W. Han, H.-S. Tae, and S.-I. Chien, "Image sticking phenomena 7 of adjacent cells induced by iterant discharged cells in 42-in. PDP TV," in *Proc. IDW Dig.*, 2003, pp. 917–920.

[5] T. Kosaka, K. Sakita, and K. Betsui, "Firing voltage fluctuation phenomenon caused by gas density nonuniformity in PDPs," in *Proc. IDW/AD Dig.*, 2005, pp. 1469–1472.

[6] L. C. Pitchford, J. Wang, D. Piscitelli, and J.-P. Boeuf, "Ion and neutral energy distribution to the MgO surface and sputtering rates in plasma display panel cells," *IEEE Trans. Plasma Sci.*, vol. 34, no. 2, pp. 351–359, Apr. 2006.

[7] C.-S. Park, H.-S. Tae, Y.-K. Kwon, S. B. Seo, E. G. Heo, B.-H. Lee, and K. S. Lee, "Experimental study on halo-type boundary image sticking in 42-in. AC plasma display panel," in *Proc. SID*, 2006, pp. 1213–1216.

[8] Y.-G. Han, S. B. Lee, C. G. Son, S. H. Jeong, N. L. Yoo, H. J. Lee, J. H. Lee, K. B. Song, B. D. Ko, J. M. Jeong, P. Y. Oh, M. W. Moon, K. B. Jung, and E. H. Choi, "An optical characteristics for image sticking in AC-plasma display panel," in *Proc. IDW/ASID Dig.*, 2005, pp. 485–488.

[9] K. Sakita, K. Takayama, K. Awamoto, and Y. Hashimoto, "High-speed address driving waveform analysis using wall voltage transfer function for three terminal and $V_t$ close curve in three-electrode surface-discharge AC-PDPs," in *Proc. SID*, 2001, pp. 1022–1025.

[10] H.-S. Tae, S.-K. Jang, K.-D. Cho, and K.-H. Park, "High-speed driving method using bipolar scan waveform in AC plasma display panel," *IEEE Trans. Electron Devices*, vol. 53, no. 2, pp. 196–204, Feb. 2006.

[11] B.-G. Cho, H.-S. Tae, K. Ito, N.-S. Jung, and K.-S. Lee, "A study on discharge stability of cost-effective driving method based on $V_t$ close curve analysis in AC plasma display panel," *IEEE Trans. Electron Devices*, vol. 53, no. 5, pp. 1112–1119, May 2006.

**Choon-Sang Park** received the M.S. degree in electronic and electrical engineering from Kyungpook National University, Daegu, Korea, in 2006, where he is currently working toward the Ph.D. degree in electronic engineering.

His current research interests include plasma physics and driving waveform of plasma display panels.

**Heung-Sik Tae** (M'00–SM'05) received the B.S., M.S., and Ph.D. degrees in electrical engineering from the Seoul National University, Korea, in 1986, 1988, and 1994, respectively.

Since 1995, he has been a Professor in the School of Electrical Engineering and Computer Science, Kyungpook National University, Daegu, Korea. His research interests include the optical characterization and driving waveform of plasma display panels, the design of millimeter wave guiding structures, and electromagnetic-wave propagation using metamaterial.

Dr. Tae is a member of the Society for Information Display. He has been serving as an Editor for the IEEE Transactions on Electron Devices section on Display Technology since 2005.

**Young-Kuk Kwon** received the B.S. degree in chemical science from Keimyung University, Daegu, Korea, in 1995, and the M.S. degree in chemical science from Kyungpook National University, Daegu, Korea, in 1997.

He is currently a Manager in the Plasma Display Panel Division, Samsung SDI Company Ltd., Cheonan City, Korea. His current research interests include plasma discharge and panel design of plasma display panels.

**Eun Gi Heo** received the B.S. degree in physical science from Seoul National University, Seoul, Korea, in 1988, and the M.S. and Ph.D. degrees from Korea Advanced Institute of Science and Technology, Taejon, Korea, in 1990 and 1996, respectively.

He is currently a General Manager with the Development Team, Plasma Display Panel Division, Samsung SDI Company Ltd., Cheonan City, Korea. His current research interests include plasma physics and panel design of plasma display panels.